Computation of Alfvén Eigenmode stability and saturation through a reduced fast ion transport model in the TRANSP tokamak transport code

M. Podestà, M. Gorelenkova, N. N. Gorelenkov and R. B. White

Princeton Plasma Physics Laboratory, Princeton NJ 08543 - USA

(Dated: January 12, 2017)

Abstract

Alfvénic instabilities (AEs) are well known as a potential cause of enhanced fast ion transport in fusion devices. Given a specific plasma scenario, quantitative predictions of (i) expected unstable AE spectrum and (ii) resulting fast ion transport are required to prevent or mitigate the AE-induced degradation in fusion performance. Reduced models are becoming an attractive tool to analyze existing scenarios as well as for scenario prediction in time-dependent simulations. In this work, a neutral beam heated NSTX discharge is used as reference to illustrate the potential of a reduced fast ion transport model, known as *kick model*, that has been recently implemented for interpretive and predictive analysis within the framework of the time-dependent tokamak transport code TRANSP [R. J. Hawryluk, *Physics of Plasmas Close to Thermonuclear Conditions*, CEC Brussels, **1**, 19 (1980)]. *Predictive* capabilities for AE stability and saturation amplitude are first assessed, based on given thermal plasma profiles only. As an example of the flexibility of the model within TRANSP, changes in the mode's behavior are discussed when neutral beam injection parameters are varied. Predictions are then compared to experimental results, and the *interpretive* capabilities of the model further discussed. Overall, the reduced model captures the main properties of the instabilities and associated effects on the fast ion population. Additional information from the actual experiment enables further tuning of the model's parameters to achieve a close match with measurements.

PACS numbers: 52.35.Bj, 52.50.Gj, 52.55.Pi

I. INTRODUCTION

Alfvénic instabilities (AEs) are known as a potential cause for increased fast ion transport in tokamaks, including future fusion reactors such as ITER [1]. A major task within the fusion community is to develop tools that enable quantitative predictions of AE-related fast ion transport in future devices based on present experiments and on results from theory and numerical codes. At present, numerical codes can predict what AE spectrum is expected for a given background discharge scenario (see, for instance, Refs. [2][3][4] and references therein). Good progress has also been made to compute fast ion transport for a given spectrum of AE instabilities. A remaining challenge is to find reliable methods to compute AE stability, the resulting saturated mode amplitudes and associated transport in time-dependent transport codes that are suitable for simulations of a whole plasma discharge. In recent years, reduced models are assuming an important role as an effective tool to distill information from theory and first-principles codes and implement methods to investigate AE stability and fast ion transport, with reduced computing time achieved at the expenses of simplified physics models [5][6][7].

This work discusses the capabilities of a physics-based, reduced fast ion transport module (known as *kick model* [8]) to provide quantitative information on AE mode stability, saturation amplitude and associated fast ion transport. The model is implemented in the time-dependent tokamak transport code TRANSP [9]. The advantage of having the kick model implemented in TRANSP is that more reliable fast ion physics can be integrated within a solid, validated framework for tokamak discharge analysis and scenario development. In this regards, the model complements physics studies performed with first-principles codes that are usually limited to single time slices and that focus of fast ion physics rather than whole-discharge simulations (e.g. including thermal plasma evolution).

To illustrate the model's capabilities, a discharge from the NSTX spherical torus [10] is taken as reference. The selected discharge features unstable toroidal Alfvén eigenmodes (TAEs) that lead to a measurable reduction in the overall performance, e.g. quantified through the deficit of the measured neutron rate with respect to TRANSP simulations that only include (neo-)classical fast ion transport mechanisms (referred to as *classical* simulations throughout the rest of the paper). Alfvénic instabilities observed on NSTX are characterized by features that make their study very relevant for benchmarking theory and numerical codes. Modes are often observed in a bursting/chirping regime [11][12], as opposed to quasi-stationary mode amplitude and frequency typically observed on other devices. Occasionally, strongly non-linear events such as TAE *avalanches*

are also observed [13][14]. In general, deviations from what can be arguably classified as 'linear' TAE physics provide validation conditions that are not commonly available from other devices, thus pushing the applicability conditions of theories and numerical models to the extremes of their range of applicability.

In the remainder of the paper, the method of analysis is first described in Sec. II, focusing on the possible applications in terms of predictive capabilities of the kick model and of its use as an interpretive tool. Examples of predictive analysis are discussed in Sec. III, in which it is shown how the unstable TAE spectrum and TAE saturation amplitude can be inferred through a power balance analysis. The results of kick model predictions are compared to actual measurements in Sec. IV. The comparison reveals some of the limitations of the model, e.g. in predicting the bursting mode amplitude evolution. However, it also indicates that predictions are in quantitative agreement with the experiment (within the model's uncertainties), thus providing a satisfactory initial validation of the model. The main results of this work are summarized in Sec. V, which concludes the paper.

II. METHODOLOGY

In recent years, the NUBEAM module [15][16] implemented in TRANSP has been updated to include a physics-based, reduced model to account for resonant fast ion transport induced by Alfvénic and other MHD instabilities. The new model, known as *kick model* [8], introduces a kick probability matrix in NUBEAM. The matrix is defined over phase-space constant of motion variables E, P_ϕ and μ that define the fast ion energy, toroidal angular momentum and magnetic moment [17]. For each (E, P_ϕ, μ) region in phase space, the matrix contains a probability $p(\Delta E, \Delta P_\phi)$ which represent the probability of correlated energy and P_ϕ kicks experienced by a fast ion as a result of its interaction with instabilities. Each probability matrix is associated with either a single mode or a set of modes. The kick matrix is computed via particle following codes such as ORBIT [18], using mode structures computed through MHD codes such as NOVA and its kinetic extension NOVA-K [19][20][21].

Kick amplitudes are scaled as a function of time according to mode amplitude waveforms, which are provided as input to TRANSP. Note that, contrary to what erroneously stated in previous works (e.g. Refs. [8][22][23]), the actual kick scaling factors used as input in TRANSP are proportional to the *square* of the mode amplitude. This can be seen by considering that kicks in NUBEAM/TRANSP are applied in terms of power, e.g. keV/s for the energy kicks. Differences

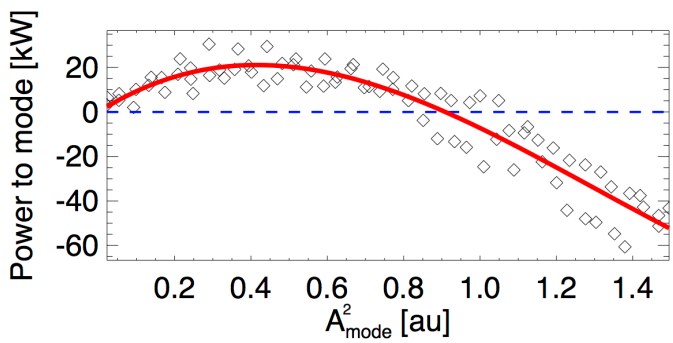

FIG. 1: Illustration of the principles for power balance analysis through the kick model in a NUBEAM/TRANSP. The power P_{EP} transferred between fast ions and each mode (or set of modes) run is recorded as a function of the mode amplitude. Regions with positive $P_{EP}(A_{mode})$ correspond to power flowing from the fast ions to the mode. Symbols are the results from TRANSP and the solid red line is a polynomial fit to the TRANSP data.

between the wrong assumption of a linear relation between mode amplitudes and kick amplitudes, as compared to the correct quadratic relation, are especially important for the small amplitude regime used to infer the *linear* mode stability (Sec. II A). In general, using the correct relation is of paramount importance whenever quantitative results are required, for instance to compare the predicted amplitudes with actual measurements (Sec. IV A).

For an interpretive run with TRANSP based on the kick model, mode amplitudes are inferred from available experimental data, e.g. from Mirnov coils or internal measurements from reflectometers, interferometers or electron-cyclotron emission (ECE) systems. Semi-predictive analysis, which is the first main topic of this work, relies on a different approach, which is based on the modeled energy exchanged between fast particles and each mode (or set of modes). Figure 1 shows the reconstructed power exchanged between fast ions and a single $n = 4$ TAE for a NSTX discharge. As the mode amplitude is increased, power flows from the fast ion population to the mode, indicating that the selected mode is driven unstable. As the mode amplitude is further increased, the power decreases as a result of modifications of the fast ion phase space regions where interactions with the mode occur. Eventually, at sufficiently large amplitude the power becomes negative indicating that net energy is now forced to flow from the mode to the particles, which in reality would imply a damping of the mode back to smaller amplitudes. This behavior is further investigated in the next Section, showing how information on mode stability and saturation can be inferred from a power balance analysis.

A. Power balance analysis: inferring growth rate and saturation amplitude

For a mode interacting with a fast particle population, the time evolution of the mode energy, E_w, can be expressed as

$$\frac{\partial E_w}{\partial t} = P_{EP} - 2\gamma_{damp}\, E_w \tag{1}$$

Here $P_{EP} = P_{EP}(E_w)$ is the power flowing from the fast ions to the mode and γ_{damp} is the mode's damping rate. A growth rate, γ_{gr}, can be introduced in Eq. 1:

$$\gamma_{gr}(E_w) \doteq \frac{P_{EP}(E_w)}{2E_w} \;\Rightarrow\; \frac{\partial E_w}{\partial t} = 2\left[\gamma_{gr} - \gamma_{damp}\right] E_w \tag{2}$$

Equation 2 can be probed through the kick model in TRANSP/NUBEAM by prescribing a modulated amplitude $A^2_{mode}(t)$ for the kicks, e.g. with a triangular waveform, and recording the corresponding power $P_{EP}(E_w)$ (Figs. 2a-b) to reconstruct the power transfer characteristic curve (Fig. 2c). (Alternatively, several runs at constant mode amplitude can be combined to reconstruct the $P_{EP}(E_w)$ characteristic for each mode).

Because of its dependence on the power exchanged between fast ions and the mode(s), the growth rate γ_{gr} is, in general, a function of the instantaneous mode amplitude A_{mode} (proportional to $\sqrt{E_w}$). However, at sufficiently small mode amplitude the effect of the mode(s) on the fast ion distribution is negligible. This low-amplitude regime is here referred to as the *linear* phase of mode growth, cf. Fig. 2c, and can be characterized by a *linear* growth rate:

$$\gamma_{lin} \doteq lim_{E_w \to 0}\, \frac{P_{EP}(E_w)}{2E_w} \tag{3}$$

Based on Eq. 2 with $\gamma_{gr} \equiv \gamma_{lin} = constant$, the mode has an initial exponential growth in time until the regions of fast ion phase space in which significant interaction occurs start to be affected by the mode(s). For sufficiently large amplitude, particles are pushed outside the interaction region. P_{EP} decreases and γ_{gr}, which is now a function of E_w in this *non-linear* phase, decreases. Eventually, saturation occurs when $\gamma_{gr} - \gamma_{damp} \to 0$ for a finite $E_w \to E_w^{sat}$.

In the limit of negligible damping, the saturation condition reduces to $P_{EP}(E_w) \to 0$ for a finite mode amplitude as shown in Fig. 2c. As a finite γ_{damp} is added, the power associated with damping scales as $P_{damp} \propto A^2_{mode}$ and the intersection point $P_{EP} = P_{damp}$ gives the saturation amplitude. Note that the assumption $P_{damp} \propto A^2_{mode}$ implies a constant γ_{damp}, e.g. from ion/electron Landau damping and continuum damping. Therefore, the method proposed herein accounts for those common wave damping mechanisms and for the wave-particle saturation mechanism [3][4]. Other

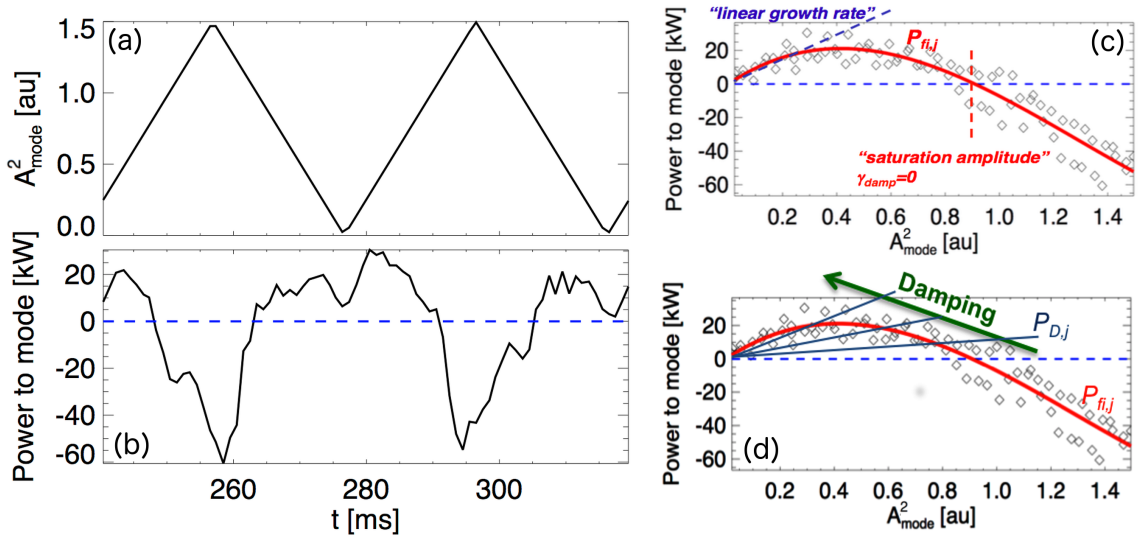

FIG. 2: Illustration of the numerical method to infer *linear* stability and saturation amplitude. (a) The mode amplitude in TRANSP is swept and (b) the corresponding power transfer between fast ions and mode recorded. (c) The $P_{EP}(A_{mode})$ characteristic is interpreted as a function of time to infer the *linear stability* in the limit $A_{mode} \to 0$ and the saturation amplitude for which $P_{EP} \to 0$ for finite A_{mode}. (d) When a finite damping rate is included, saturation amplitude is identified from the balance between P_{EP} and the power corresponding to that damping rate. In practice, this leads to smaller saturation amplitudes as the damping rate increases.

mechanisms are not included, namely non-linearities associated with wave-wave coupling which are expected to become important as the mode amplitudes become sufficiently large [4][24][25][26]. At present, the latter mechanisms can only be introduced by modifying the input mode amplitude waveforms, as discussed in Sec. IV B.

B. Predictive capability of kick model analysis

Based on the interpretation of the power balance from Eqs. 2-3, the predictive capability of the kick model analysis can be assessed. Four degrees of predictability can be defined based on the available information on instabilities:

1. *Interpretive analysis.* If sufficient experimental data are available on the unstable mode spectrum and the amplitude evolution of each mode, the kick probability matrices and mode amplitude evolution can be reconstructed directly. From the measured spectrum, the radial mode structure can be obtained by comparing internal measurements (e.g. from ECE or reflectometers) with results from a MHD eigenmode solver such as NOVA. The

mode structure is then used in ORBIT to compute the transport matrices for a nominal mode amplitude value, e.g. A_{mode}=1. The whole time-dependent $A_{mode}(t)$ is inferred from re-scaled experimental measurements. The power output $P_{EP}(A_{mode})$ from TRANSP for each mode, along with comparison with other measurements such as neutron rate, total stored energy or data from other diagnostics [27], can then be used *a-posteriori* to check the consistency of the initial assumptions.

2. *Semi-interpretive analysis.* In most experiments, data on mode structures and their temporal evolution are incomplete. For instance, the unstable mode spectrum may be known from Mirnov coil measurements at the plasma edge, but the radial mode structure is not directly measured. Partial experimental information can be used to select candidate modes (e.g. from NOVA analysis) based on mode number and frequency. Next, edge measurements can provide an initial guess for the mode amplitude, but uncertainties remain because of the radial localization of different modes that can affect the actual signal amplitude from the coils. Equation 2, the damping rate provided by NOVA and other measurements such as neutron rate and stored energy are then used to refine the mode amplitude(s) evolution vs. time in iterative TRANSP runs.

3. *Semi-predictive analysis.* In cases for which background profiles of the thermal plasma evolution are known but no *a-priori* information or measurements on the mode activity is available, both mode radial structure (hence, kick probabilities) and amplitude(s) need to be inferred from a *post-hoc* analysis. The first step is to obtain candidate modes from NOVA, and compute the associated transport probabilities from ORBIT assuming a nominal mode amplitude $A_{mode} = 1$. Then, linear stability is gauged through the kick model as discussed in Sec. II. The most unstable modes are thus selected. Additional TRANSP runs with larger mode amplitude provide the expected saturated amplitude(s).

4. *Predictive analysis.* When prediction and development of scenarios is performed, no information is available on either thermal plasma evolution and instabilities. TRANSP simulations can be used for time-dependent scenario development, but - at present - self-consistent predictions (within TRANSP and its modules) of unstable mode spectrum and amplitudes is not implemented. This would require the implementation of two main elements, namely (i) a MHD eigenmode solver and (ii) a mode stability module. Instead, what is now achievable is an iterative approach in which thermal profiles are first predicted through TRANSP, then

used to compute the expected mode spectrum from NOVA - which provides the input for computing the transport probabilities and damping rates. The following analysis follows the prescription for *semi-predictive* analysis, with the caveat that iterations on the simulated thermal profiles may be required since fast ion transport - hence, pressure - influences the overall equilibrium.

In practice, the boundary between different types of analysis may not be well defined. For instance, the target of *predictions* need to be defined - whether it is the mode evolution (as assumed in the discussion above), or the match with measured quantities such as neutron rate or other quantities.

C. Open issues and major sources of uncertainties

Each of the approaches discussed in Sec. II B is subject to uncertainties. Some of them are common to other approaches for computing mode stability, whereas others are specific to the kick model assumptions and analysis procedure.

Arguably, the main source of uncertainties in computing mode stability for a given scenario is the identification and selection of the candidate mode structures. For each toroidal mode number n included in the analysis, codes such as NOVA output all eigenmode solutions, regardless of their actual stability and of the mode type (e.g. toroidal or reversed-shear AEs). The selection of the actual mode spectrum in terms of n and frequency introduces some degree of arbitrariness. Even when the growth rate computed through the kick model is used to select the most unstable modes, there can be cases for which several modes with the same n are equally valid candidates. As will be shown in Sec. III, this may conflict with actual data showing only one mode destabilized at each n for specific experimental conditions. In this case, the ambiguity is between selecting the most unstable mode for each n or the mode that features the largest saturation amplitude.

Further, ideal MHD codes such as NOVA search for *local* eigenmode solutions as a function of radius. When the radial mode structure intersect an AE continuum, the local solution can have a discontinuity that is not resolved by ideal MHD. An example is shown in Fig. 3, in which the radial structures of two $n = 4$ modes with close frequencies are shown. Both modes intersect the lower TAE continuum around $\Psi_{pol} \approx 0.3 - 0.35$ (Ψ_{pol} is the poloidal flux). The discontinuity in the computed poloidal harmonics results in a sudden jump (sign inversion) of the harmonics' phase. Of the two modes, the one in Fig. 3a has maximum amplitude far from the discontinuity, so it can be assumed that its radial structure is overall well resolved. The mode in Fig. 3b peaks near

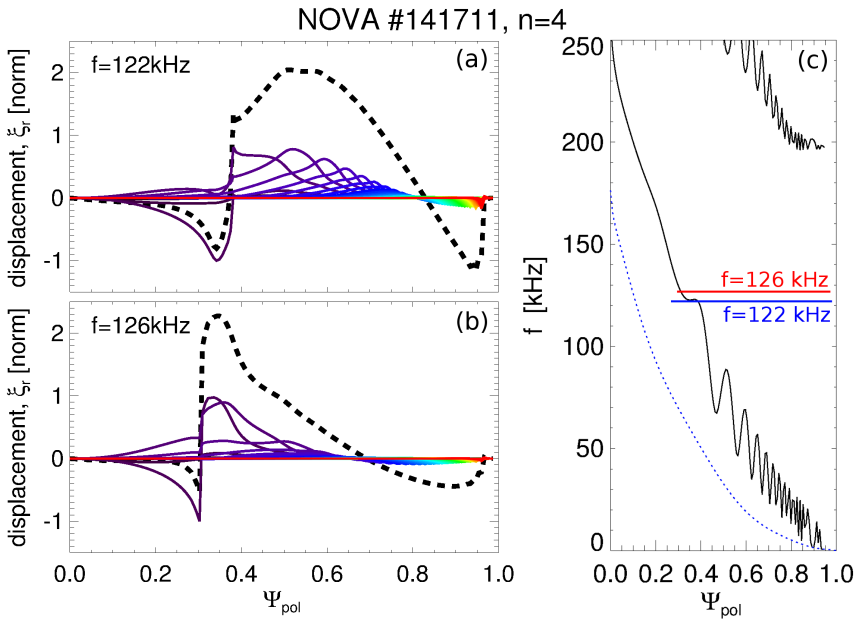

FIG. 3: Examples of radial eigenmode structures computed by NOVA for $n = 4$ TAE modes. Both modes in (a) and (b) intersect the lower TAE continuum and a discontinuity is observed in the poloidal harmonics (colored lines). The total mode structure in panel (a), shown as which dashed line, has a maximum far from the discontinuity and is considered as a valid solution. Instead, the mode in panel (b) peaks near the discontinuity and is considered as 'unphysical'. (c) TAE continuum vs poloidal flux, Ψ_{pol}. Frequency location of the two modes are shown as red and blue lines.

the discontinuity, so ambiguity remains in whether this solution is acceptable or polluted by the discontinuity. In practice, modes from NOVA are rejected from the possible solutions if the *total* mode structure peaks at the intersection with the continuum.

Damping rates used in Eq. 2 are computed through the NOVA code and its kinetic extension NOVA-K. In the following, only three contributions to the total γ_{damp} are retained, namely electron/ion Landau damping and continuum damping. Validity of the NOVA formulation for other damping mechanisms, such as radiative damping [28], is arguable in the limit of small aspect ratio and strong mode interaction with the Alfvén continuum to which this work applies. Those other damping terms are neglected in the following discussion, implying that γ_{damp} is a lower limit estimate of the total damping. As a consequence, the inferred saturation amplitude must be considered as an upper limit.

The sources of uncertainty discussed above are common to all codes and analysis methods relying on ideal MHD calculations of the mode structure. For the kick model analysis, the discontinuity at intersection with the continuum introduces additional uncertainty. Consider the saturation

condition from Eq. 2, which can be cast as the balance between power transferred from the fast ions to the mode and the overall power damped by the mode, $P_{EP} = P_{damp}$ with $P_{damp} \doteq 2\gamma_{damp} E_w$. The electromagnetic energy associated with each mode, E_w, is computed for a nominal amplitude $A_{mode} = 1$ by integrating the perturbation over the plasma volume, V:

$$E_w = \frac{1}{4\pi\,\mu} \int_V \delta B^2(\mathbf{x}) d\mathbf{x} \tag{4}$$

The perturbed field δB is inferred from the α coefficients associated with the perturbation [17]:

$$\delta \mathbf{B} = \nabla \times \alpha \mathbf{B} \tag{5}$$

Although the radial perturbation of the B field is mostly responsible for fast ion transport, all three $\delta\mathbf{B}$ components must be taken into account to compute the total mode energy. Therefore, the integral in Eq. 5 will contain terms proportional to partial derivatives of α along Ψ_{pol}, which lead to divergent terms if $\alpha = \alpha(\Psi_{pol})$ is discontinuous. In this work, this issue is resolved by eliminating narrow regions across the intersection with the continuum when computing Eq. 4. Based on the width of the excluded region, the resulting mode energy E_w can vary by $\pm 20\%$. Given the large variability of $P_{EP}(A_{mode})$ shapes found for different modes, the uncertainty that propagates to the calculation of mode saturation from Eq. 2 (also cf. Fig. 2) must be evaluated for each mode.

III. KICK MODEL PREDICTIONS FOR A NSTX DISCHARGE

In this Section, the kick model analysis introduced in Sec. II is applied to a L-mode scenario with Neutral Beam injection on the NSTX spherical torus [10]. The target scenario is first introduced in Sec. III A, then kick model results for mode stability, saturation amplitude and resulting fast ion transport are discussed in Secs. III B-III C. Results obtained in these Sections can be classified as *semi-predictive*, according to the classification introduced in Sec. II B. Direct comparison with experimental data, and the associated *semi-interpretive* and *interpretive* analyses, provide additional insight about the capability and limitations of the model. Comparison with the experimental NSTX results and additional kick model analysis are presented in Sec. IV.

A. Target scenario

The selected NSTX discharge #141711 (Fig. 4) has a toroidal field ~ 0.5 T, with density $\approx 4 \times 10^{19}$ m^{-3} during the time of interest $380 < t < 520$ ms. Electron and ion temperatures

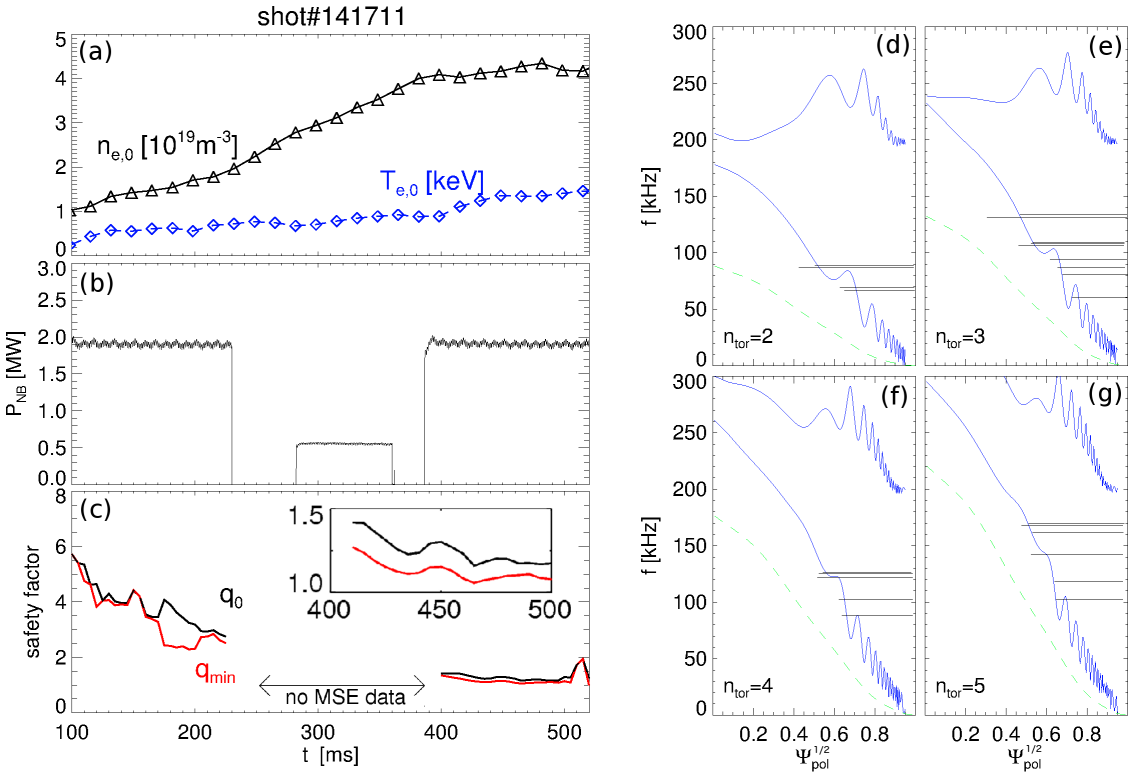

FIG. 4: Target NSTX scenario for this work (NSTX discharge #141711). (a) Electron density and temperature vs time. (b) Injected NB power. (c) Values of central and minimum of the safety factor, $q(r)$, reconstructed through the LRDFIT code constrained by MSE measurements. The inset shows details for the time range considered in this work, $380 \leq t \leq 520$ ms. (d-g) NOVA results at $t = 470$ ms for TAE continuum (blue lines) and eigenmodes for $n = 2 - 5$ with frequency $f = 50 - 200$ kHz (horizontal black lines) as a function of the poloidal flux variable, Ψ_{pol}. Dashed lines show the Doppler shift frequency from plasma rotation.

are $T_e \approx T_i \approx 1$ keV. Central plasma rotation is $f_{rot} \approx 25 - 40$ kHz. The injected NB power is $P_{NB} = 2$ MW from a single NB source with injection energy $E_{inj} = 90$ keV.

The reversed-shear safety factor, $q(R)$, evolves in time (Fig. 4c). Its minimum, q_{min}, decreases from 1.5 to ≈ 1 at the time of interest. The safety factor is reconstructed from the Grad-Shafranov equilibrium code LRDFIT [29], constrained by measurements from a Motional Stark Effect system [30]. Profiles of electron/ion density and temperature are obtained from Thomson scattering [31] and charge-exchange recombination spectroscopy [32] diagnostics covering the entire minor radius. Time resolution of the two systems is 16 ms and 10 ms, respectively.

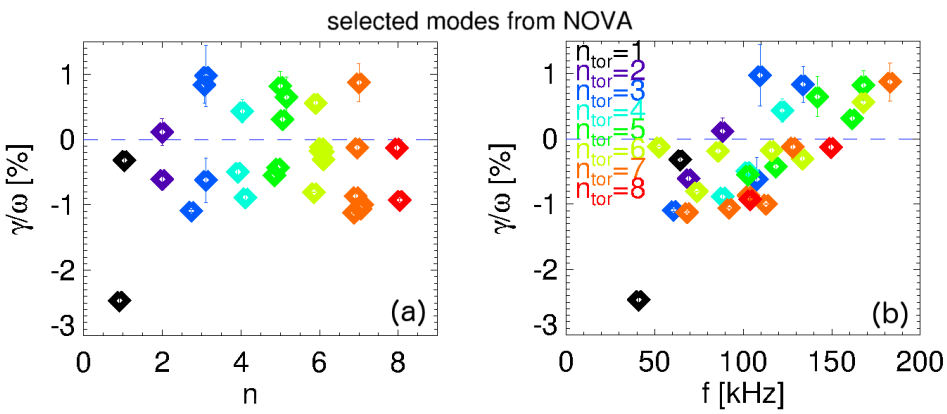

FIG. 5: Inferred net growth rate for NSTX discharge #141711 from TRANSP and kick model stability linear analysis. Rates are averaged for $450 \leq t \leq 480$ ms and vertical bars indicate the variation over that time range. Damping rate is computed by NOVA and NOVA-K. (a) Net growth rate vs toroidal mode number n. (b) Net growth rate vs frequency.

B. Prediction of unstable spectrum and saturated amplitudes

NOVA analysis is performed for the scenario in Fig. 4 based on profiles at $t = 470$ ms. The search frequency range is $50 - 200$ kHz, which covers the TAE/RSAE continua, for toroidal mode numbers $n = 1 - 8$. Details on the analysis procedure can be found in Refs. [12][13][33].

From the NOVA analysis, about 50 candidate eigenmodes are extracted. As explained in Sec. II B, the following step for semi-predictive analysis consists in running TRANSP with the selected modes to infer the *linear* mode stability. The results for the net growth rate (difference between growth rate and damping from NOVA) are shown in Fig. 5. Of the original eigenmodes, only nine modes are found unstable with net growth rates $\gamma/\omega \lesssim 1\%$. The unstable spectrum is limited to $n = 2 - 7$, whereas $n = 1, 8$ modes are stable. The frequency range is $70 - 180$ kHz.

In Fig. 6, stability results from the kick model are compared with those from the post-processor NOVA-K [19], which computes stability including finite Larmor radius (FLR) effects [21]. Following the procedure described in Ref. [33], the fast ion population is modeled as superposition of three slowing-down distributions representing the three energy components of the injected NB ions. Each component is weighted by the corresponding β (ratio of kinetic to magnetic pressure) computed by TRANSP. An additional run is performed to compute ion Landau damping for the actual ion temperature and including finite plasma rotation.

Figures 6a-b show the comparison of net growth rate (including damping) and growth rate only when FLR effects are neglected in NOVA-K. Since both models use the same damping rates

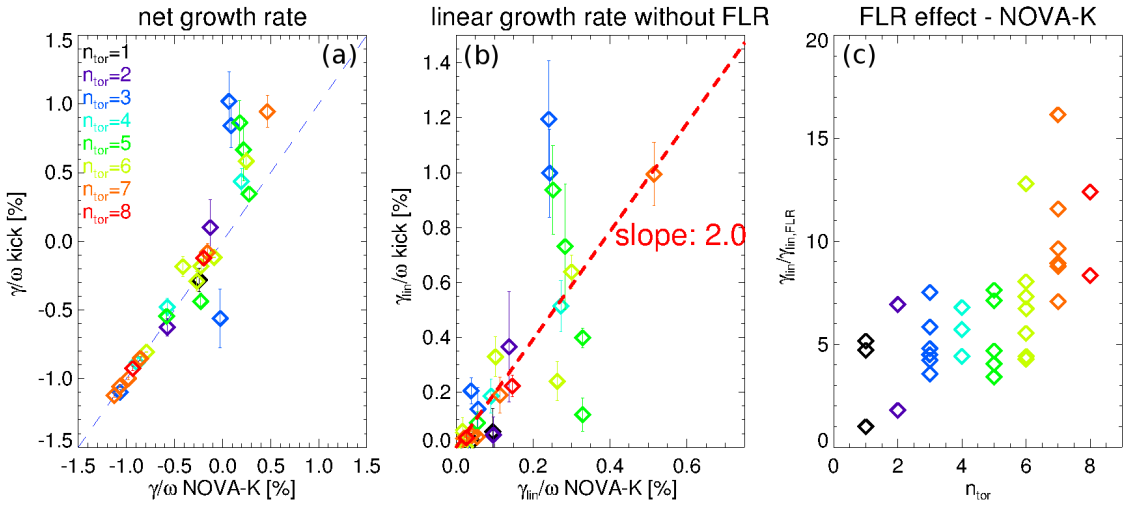

FIG. 6: Comparison of TAE stability obtained from kick model and NOVA-K. For the kick model, rates are averaged for $450 \leq t \leq 480$ ms and vertical bars indicate the variation over that time range. (a) Net growth rates for $n = 1 - 8$. Results from the two models converge for decreasing γ/ω since the same damping rates (from NOVA-K) are used in both cases. (b) Linear growth rate with no FLR effects included in NOVA-K. (c) Ratio of growth rate from NOVA-K without and with FLR effects as a function of toroidal mode number.

computed by NOVA, the net growth rates converge for values approaching zero and becoming negative. A larger spread is found for positive growth rates, for which the contribution of the NB ion drive becomes non-negligible. Overall, the two models agree within a factor ~ 2, although differences up to a factor four are obtained for some of the modes. Considering the simplifications adopted in the kick model, the intrinsic difference on how the fast ion distribution is modeled and the different treatment of fast ion sources and sinks (which are absent in NOVA-K) for the two models, the level of agreement can be considered satisfactory. Note that TAE stability for this same NSTX discharge has been previously investigated by White *et al.* in Ref. [34] (see Table 1 and Fig. 17) by using the ORBIT code. As for the present kick model analysis, mode structures and damping rates were inferred from NOVA/NOVA-K. Since different assumptions on the magnetic equilibrium were used in that work, a direct comparison between growth rates from ORBIT and from the kick model is not possible. However, the main conclusions from Ref. [34] are confirmed for the kick model analysis as well, namely results are extremely sensitive to the choice of damping rates and of the input fast ion distribution.

Much larger discrepancies appear in the computed growth rates when finite Larmor radius effects are included in NOVA-K (see Fig. 6c), resulting in a reduction of $2 - 15$ in the linear growth

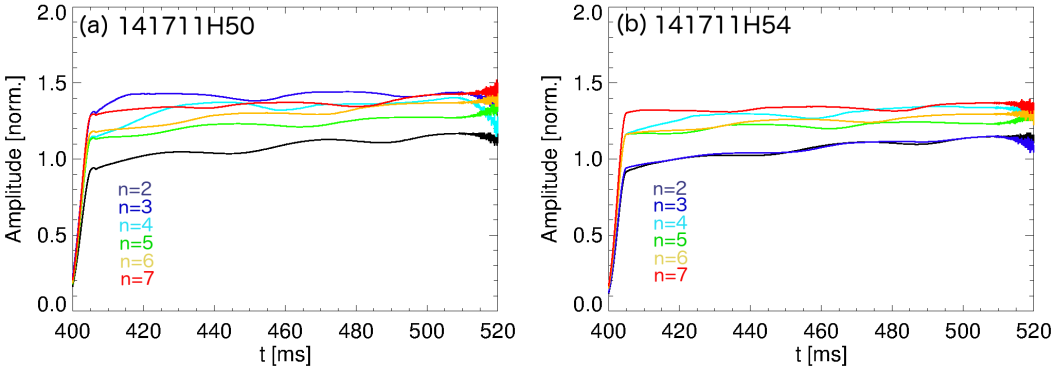

FIG. 7: Inferred saturated mode amplitudes vs time for NSTX #141711. Amplitudes are computed assuming damping rate from NOVA-K. Panels refer to two different selections of unstable modes: (a) most unstable mode for each toroidal mode number or (b) mode spectrum that more closely matches the experimental spectrum.

rate depending on the specific mode and its radial structure. FLR effects are not included in the kick model, which is based on analysis with the gyro-center code ORBIT. Therefore, it can be assumed that the kick model tends to over-estimate the growth rate. As a test, FLR effects can be approximated in ORBIT by averaging the perturbation around the nominal gyro-center position for each particle, based on its Larmor radius. Initial results for a limited set of modes indicate a reduction in the γ_{lin}/ω from the kick model that is consistent with NOVA-K predictions. The relevance of FLR effects in these predictions is further discussed in Sec. IV A based on experimental measurements of the unstable mode spectrum.

Once the most unstable modes are selected, they are divided into two sets to investigate their amplitude saturation level, see Fig. 7. The first set includes the most unstable modes with $n = 2-7$. In the second set, the second most unstable modes are used for those n's that result in more than one unstable mode. In subsequent TRANSP runs, mode amplitudes are swept around the reference value $A_{mode} = 1$ for each mode, which corresponds to perturbations with peak $\delta B_r/B_0 = 5 \times 10^{-4}$ (δB_r is the radial component of the perturbed magnetic field). Once the actual damping rates from NOVA are taken into account, the analysis results in roughly similar amplitudes, $A_{mode} \sim 1 - 1.5$ for both set of modes . To test the model sensitivity to the assumptions on damping rate, the same analysis is performed assuming a constant damping $\gamma_{damp}/\omega = 1\%$ for all modes, which results in an average reduction of the mode amplitudes by $\sim 30\%$.

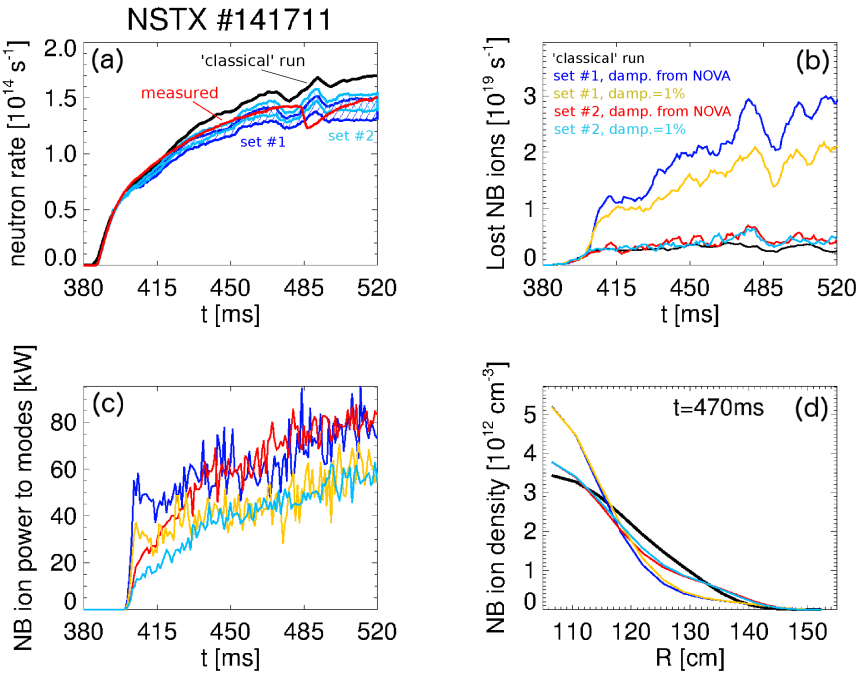

FIG. 8: TRANSP predictions using the two sets of modes and amplitudes from Fig. 7. (a) Neutron rate, showing the measured values (red curve), predictions for TRANSP run with *classical* fast ion transport (black). Predictions from the kick model assume damping rates from NOVA-K (lower curves for each run) and a constant $\gamma_{damp} = 1\%$ (upper curves). (b) Computed fast ion losses. (c) Total power transferred from fast ions to the modes, P_{EP}. (d) Radial fast ion density profiles at $t = 470$ ms.

C. Predictions of fast ion transport caused by instabilities

The unstable modes and their saturation amplitude identified in Sec. III B can be used in TRANSP to predict the expected level of fast ion transport, knowing the background plasma profiles and the NBI settings. The results are shown in Fig. 8.

For both sets of unstable modes the kick model predicts a reduction in neutron rate of $5 - 10\%$ with respect to *classical* TRANSP simulations, depending on the damping rate used to infer the saturated mode amplitudes (values from NOVA vs. constant $\gamma_{damp}/\omega = 1\%$). These values are consistent with the measured neutron rate deficit, which increases from ≈ 0 as the NB injection starts up to $\approx 10\%$ in the later part of the discharge. (The large, sudden drop around $t = 485$ ms is caused by a TAE avalanche and is not considered in this Section).

The amount of NB ion losses is shown in Fig. 8b. Losses up to six times the value computed for the *classical* TRANSP run are computed when the damping rate from NOVA is used (cf. runs $H50$ and $H54$). The assumption of constant damping $= 1\%$ brings the losses down near the classical

level (runs $H51$ and $H55$) as a result of the reduction in mode amplitude.

In contrast with the different level of NB ion losses, the power transferred from fast ions to the modes is less sensitive to the assumptions on the damping rate but varies between the two sets of modes, see Fig. 8c. This result is not general but depends on the relation $P_{EP} = P_{EP}(A_{mode})$ for the different modes and for a given set of NBI parameters. Referring to Fig. 2c-d, the different levels of damping rate span a relatively flat region around the maximum of $P_{EP}(A_{mode})$ for this specific case, thus resulting in little variations in the total power transfer in spite of the larger variations in saturation amplitude.

Similar differences are observed in the predicted fast ion radial profiles, see Fig. 8d, which are nearly independent of the assumed γ_{damp} but vary considerably for the two sets of modes. One clear feature that emerges from Fig. 8d is the tendency of the computed profiles to peak near the magnetic axis with respect to the reference, *classical* TRANSP run. This feature is further discussed in Sec. IV B based on actual experimental measurements.

D. Numerical experiments on mode stability

One of the benefits of the kick model implementation in NUBEAM/TRANSP is the possibility to perform *numerical experiments*, e.g. to investigate the sensitivity of the predicted results on the initial assumptions or to develop new scenarios starting from a given reference case. This is especially important when fast ion behavior is considered in the broader context of a tokamak discharge including both the effects of fast and thermal particles, for instance to evaluate NB current drive or - in general - transport and power balance.

In this Section, an example of scenario development is discussed. Consider the scenario in Fig. 4. The analysis discussed in Secs. III B-III C indicates that TAEs are expected to be unstable, with moderate loss of performance as inferred, for example, from the reduction in neutron rate. One question that arises is whether a different NB injection geometry can be effective in mitigating - or suppressing - the enhanced fast ion transport caused by TAEs by reducing the mode's drive. This exercise is of practical utility as NSTX has completed a major upgrade to NSTX-Upgrade [35], of which one of the major elements has been the addition of a second NB line with more tangential injection.

Figure 9 shows the predicted variation of the net γ/ω for the most unstable modes in Fig. 5 as the NB injection is moved from more perpendicular, $R_{tan} = 50$ cm (R_{tan} is the NB tangency radius), to more tangential and off-axis, $R_{tan} = 130$ cm. (As a reference, the magnetic axis is at

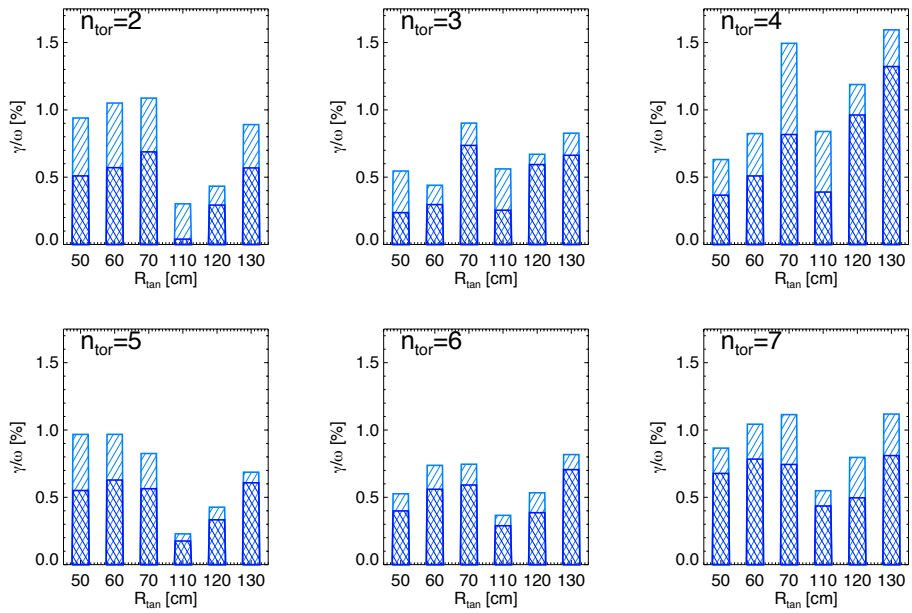

FIG. 9: Results of net growth rate, γ/ω, for toroidal mode numbers $n = 2 - 7$ assuming NB injection from sources with different tangency radius, R_{tan}. The two values for each R_{tan} correspond to the computed maximum/minimum rates for the time interval $450 \leq t \leq 470$ ms.

$\approx$ 105 cm). For these conditions, the results indicate that the three sources injecting inside the major radius have a similar effect on the modes, with only a slight increase in γ/ω for the less perpendicular source ($R_{tan} = 70$ cm). The latter is the NB source used in the actual discharge. The new NB sources installed on NSTX-U have a larger effect, with the on-axis source ($R_{tan} = 110$ cm) providing the minimum drive for the modes. Drive is increased to levels comparable to that from the perpendicular sources for the outermost, more off-axis source.

The set of diagnostics implemented in NUBEAM/TRANSP is crucial to investigate the results from this numerical NB tangency radius scan. Figures 10a-b show the NB deposition and fast ion density profiles computed by TRANSP for the different NB sources. The profiles indicate that, for these experimental conditions, only small differences can be expected among the more perpendicular sources with $R_{tan} = 50 - 70$ cm. In spite of this, some of the modes respond quite differently, as inferred from the P_{EP} power that varies by a factor ~ 2.5 (see Fig. 10e) consistently with the γ/ω results shown in Fig. 9. Other modes show negligible differences in P_{EP} and its radial profile, see Fig. 10f. The new NB sources ($R_{tan} = 110 - 130$ cm) appear to have a larger relative effect on all the modes, which can in part be explained by the large variation in deposition profile and resulting fast ion density. When combined with the γ/ω results, the variability in mode

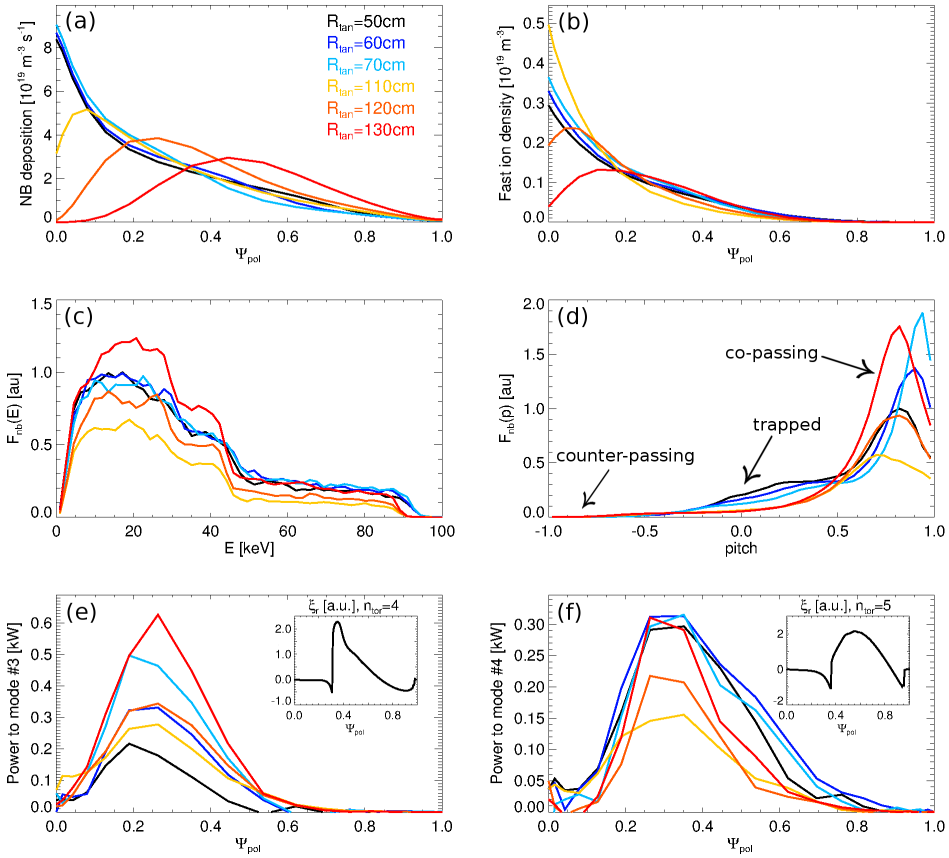

FIG. 10: Profiles for the numerical NB scan through TRANSP, averaged over $450 \leq t \leq 470$ ms. (a) NB deposition profile. (b) Radial fast ion density profile. (c-d) Fast ion distribution around $\Psi_{pol} = 0.5$ as a function of energy and pitch (pitch: ratio of parallel to total velocity). (e-f) Radial profile of power transferred from fast ions to the $n = 4, 5$ modes for the different NB sources. The insets show the radial mode structure for each mode.

response to different NBI parameters suggests that the so-called *universal drive* for TAEs associated with the radial gradient of the fast ion density is not the only factor that affect TAE stability. For the case studied in this work, stability cannot be simply explained by changes in the (average) radial gradient, or by the overlap between deposition profile and radial mode structure (shown in the inset in Figs. 10e-f). In fact, previous works have confirmed the complex role played by fast ion response to the modes in phase space rather than in configuration space or simply in the radial coordinate (see, for example, Refs. [12][23][36][34] and references therein). For example, Figs. 10b-c show the integral of the fast ion distribution around $\Psi_{pol} = 0.5$ as a function of energy and pitch (ratio of parallel to total velocity), respectively. From the figures, it results that the innermost NB sources feature a similar energy dependence, but fast ions are distributed differently as a function of pitch. In particular, co-passing and trapped regions are populated differently, which can result

in a different response of the modes depending on the location of the wave-particle resonances. The three outboard NB sources show a simpler dependence on R_{tan}, with most particles in the co-passing region and a clear increase of the fast ion density as R_{tan} shifts from the core to mid-radius. This regular behavior is sufficient to explain the trend in the response of both modes in Figs. 10e-f.

Besides the simple example illustrated above, other numerical experiments are enabled by the accurate fast ion physics contained in TRANSP/NUBEAM and by the recent implementation of the kick model in NUBEAM and can assist in the interpretation of experimental results. A partial list includes a more accurate study of FLR effects, for instance by varying the toroidal field at constant NB injection energy to vary the Larmor radius; the study of the effects of (classical) collisions on the overall mode stability and saturation by varying electron/ion density and temperature to modify slowing down time and scattering rate [37]; the characterization of phase-space resolved fast ion transport by analyzing the dynamical response of the fast ion distribution to NB modulation [27][38][39]. These potential applications of the model will be further explored in future studies.

IV. COMPARISON OF TRANSP RESULTS WITH EXPERIMENTAL MEASUREMENTS

The results obtained from the *semi-predictive* kick model analysis in Section III are here expanded to include information that is available from the real experiment. This is done to (i) assess the validity of the predictions against the actual experiment and (ii) to illustrate the additional insight that can be gathered using the model in *interpretive* mode.

A. Unstable frequency spectrum and saturated mode amplitude

The first comparison between model and experiment focuses on the instability spectrum. Figure 11 shows the spectrum of magnetic fluctuations measured by a Mirnov coil located at the vessel wall on the lo-field side. The toroidal mode numbers are also indicated in the figure. Dominant TAEs observed in the experiment have $n = 3, 4$, although a rich spectrum with $n = 2 - 6$ is observed. The measured TAE modes feature bursty amplitude as a function of time, with relative frequency variations (or *chirps*) of the order $\delta f/f \sim 10\%$ or smaller (see inset in Fig. 11). Occasionally, weak $n = 1$ activity is also detected. This coincides with times at which multiple modes have significant amplitude. Previous work has indicated that the observed $n = 1$ activity

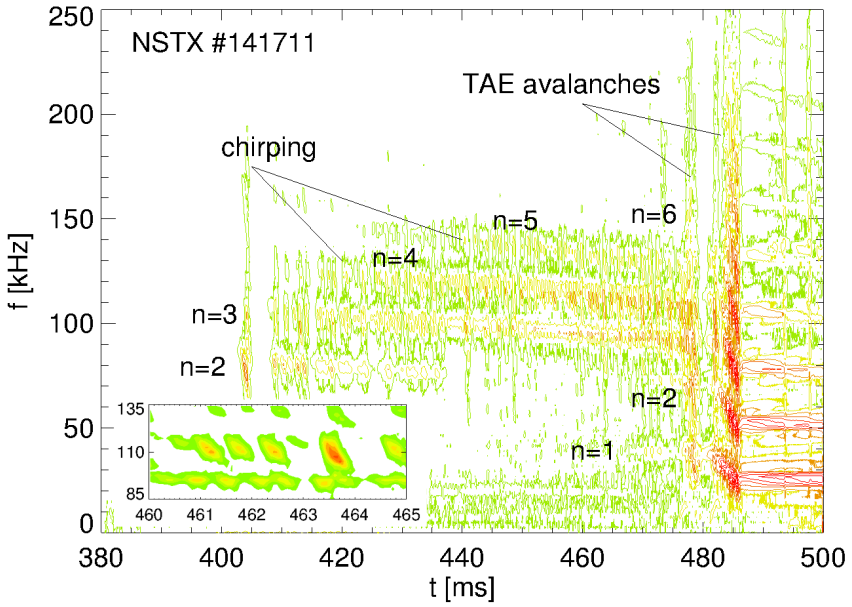

FIG. 11: Measured spectrum of magnetic fluctuations from a Mirnov coil for NSTX discharge #141711. Toroidal mode numbers are indicated by labels for each mode. The inset shows a detail of the evolution of bursting/chirping modes. Mode amplitude in the figure is increasing for colors from green to red.

is the result of three-wave coupling between pairs of TAEs with adjacent toroidal mode numbers and $n = 1$ kink-like activity, cf. Refs. [11][12]. The measured spectrum changes dramatically for $t \geq 485$ ms, when a TAE *avalanche* is destabilized. The following analysis focuses on the phase of weak bursts, neglecting the strongly non-linear avalanche event.

A time slice of the measured fluctuation spectrum for $465 \leq t \leq 475$ ms is shown in Fig. 12 and compared with kick model and NOVA-K predictions. NOVA-K analysis has been performed using the profiles at $t = 470$ ms as input. The experimental spectrum shows a rich variety of modes, with TAEs being the dominant component followed by weaker $n = 1$ activity at frequencies $f = 20 - 50$ kHz. Small amplitude, higher-n fluctuations - tentatively classified as edge harmonic oscillations [40] - are also observed at $f \leq 25$ kHz.

The unstable spectrum from kick model analysis (Fig. 12b) contains TAEs only. The $n = 1, 8$ TAEs are found to be stable and are absent from the spectrum. The sequence of dominant TAEs with $n = 2 - 7$, whose frequency increases with the toroidal mode number, appears consistent with the experimental spectrum once a frequency shift of $\approx 10 - 20$ kHz is applied. The origin of this systematic frequency shift is not yet understood, although it is noted that a similar discrepancy was found for the same scenario using the M3D-K code [41]. A candidate explanation is the specific choice of adiabatic heat index used in NOVA.

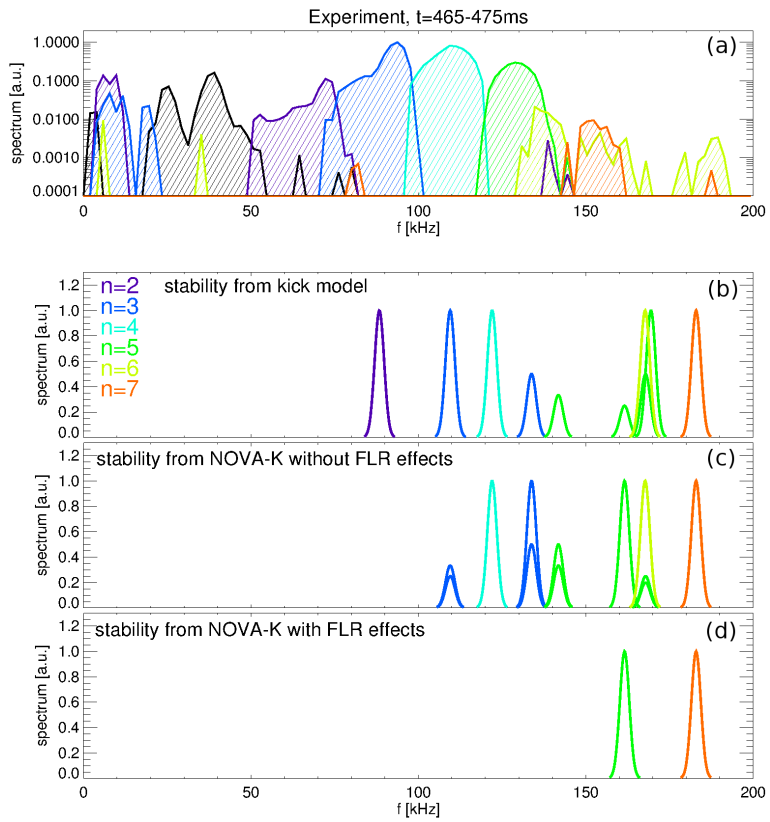

FIG. 12: Mode number spectrum from experiment (a) and comparison with stability results from kick model (b) and NOVA-K without (c) and with (d) inclusion of finite Larmor radius (FLR) effects. For panels (b-d), most unstable modes are shown with amplitude = 1, the second most unstable modes have amplitude = 0.5 and the least unstable modes have amplitude = 0.33. Colors refer to different toroidal mode numbers according to the labels in panel (b).

The NOVA-K predictions for the unstable spectrum (Figs. 12c-d) resemble those from the kick model if no FLR corrections are taken into account. The only exception is that the $n = 2$ TAE is predicted to be stable. If FLR effects are considered, NOVA-K appears to under-estimate the growth rate for most modes and only $n = 6, 7$ TAEs are found unstable. It is speculated that one reason for the reduced growth rate may be the presence of a singularity in the mode structures at the intersection with the lower TAE continuum (cf. Fig. 3). The singularity introduces a phase shift (i.e. a sign inversion) in the radial structure. Since the maximum mode amplitude is often located near the singularity, orbit smearing near the maximum by FLR effects would average over regions of opposite amplitude, thus leading to a strong (but unphysical) reduction in the estimated growth rate.

The second comparison between kick model predictions and the actual experiment refers to the

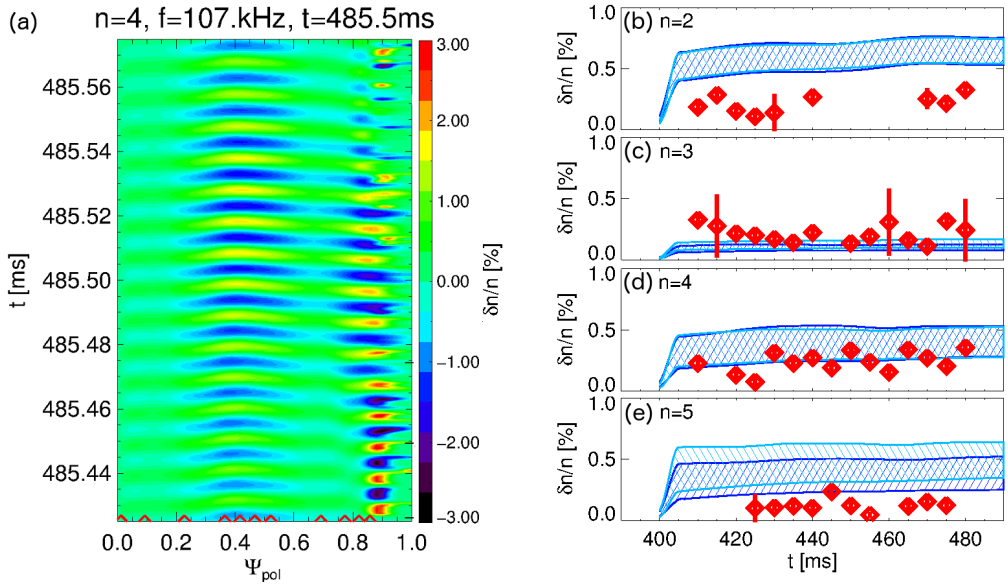

FIG. 13: (a) Example of relative density perturbation, $\delta n/n$, inferred from reflectometer's measurements for a $n = 4$ TAE mode. Symbols on the x-axis indicate the measurements position. Maximum of the fluctuation is computed for $0 \leq \Psi \leq 0.7$, removing edge regions for which the inferred $\delta n/n$ is unreliable. (b-e) Comparison between measured (symbols) and predicted (hashed regions) density fluctuations. As in Fig. 7, kick model results from two set of modes are shown with light/dark blue. For each set, amplitude is computed assuming damping rates from NOVA-K and for a constant value $\gamma_{damp}/\omega = 1\%$.

mode saturation amplitude, cf. Fig. 7. Experimentally, an array of reflectometers [42][43] is used to measure the local density fluctuations, $\delta n/n$. Analysis of reflectometer data follows the method first proposed in Ref. [12] to infer the density perturbation evolution over the short time-scale of a TAE burst. An example is shown in Fig. 13a for the $n = 4$ TAE observed in the NSTX discharge #141711. For the comparison with the kick model results, analysis is performed every 5 ms from 410 ms to 490 ms and $\delta n/n$ is inferred for each mode with sufficiently large signal-to-noise, $n = 2 - 5$.

Values of $\delta n/n$ from the kick model and the experiment are compared in Figs. 13b-e. Overall, the kick model provides reasonable predictions, usually within a factor two with respect to the experimental values. A general trend is that the kick model tends to over-predict the density perturbation, suggesting that the predicted mode amplitudes are larger than the actual ones.

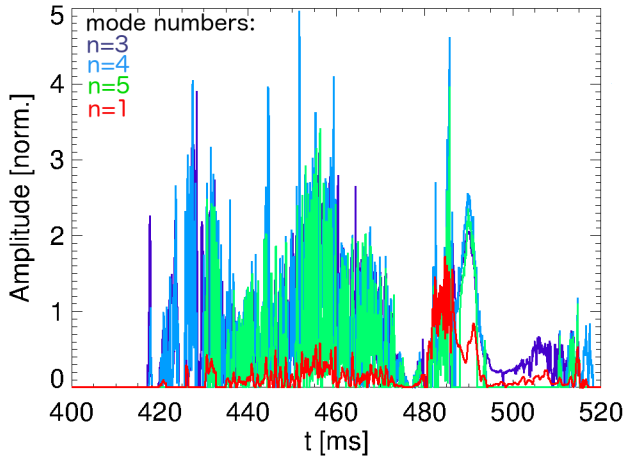

FIG. 14: Example of mode amplitudes inferred from the experimental data and rescaled by kick model (saturation) predictions. Amplitudes represent the evolution of bursting/chirping modes, including a $n = 1$ marginally stable kink-like perturbation.

B. Model tuning for interpretive analysis

The additional information from the experimental spectrum can be used to further tune the kick model parameters to achieve a better match with the experiment. As a first step, the experiment indicates that mode amplitudes are not quasi-stationary, as originally assumed e.g. in Fig. 7, but feature repetitive bursts as time evolves. The amplitude evolution for each toroidal mode number can therefore be inferred from the measurements, and then re-scaled based on the saturation amplitudes previously computed through the kick model. (As an alternative, mode behavior can be tested according to the theory presented in Ref. [44] to check whether the modes are expected to feature quasi-stationary amplitude or bursting/chirping behavior).

As a second step, the information on three-wave coupling processes present in the experiment [12] is used to mimic the presence of a time-dependent $n = 1$ component. The $n = 1$ amplitude is here computed by taking the product of the $n = 2-7$ amplitudes, then re-scaling the overall values based on a average ratio between $n = 1$ and $n = 2 - 5$ amplitudes from the measured spectrum.

A further step in this interpretive analysis is to iterate on the $A_{mode}(t)$ waveforms based on a target quantity (or more, if available) such as the measured neutron rate. An example of the iterated mode amplitudes for $n = 3 - 5$ is shown in Fig. 14. Amplitude bursts are clearly visible. Also shown is the $n = 1$ amplitude, which is only $\lesssim 10\%$ of the other amplitudes on average. The peak of $n = 1$ amplitude around $t = 485$ ms reflects the fact that all amplitudes for $n = 2-7$ spike simultaneously during the TAE avalanche.

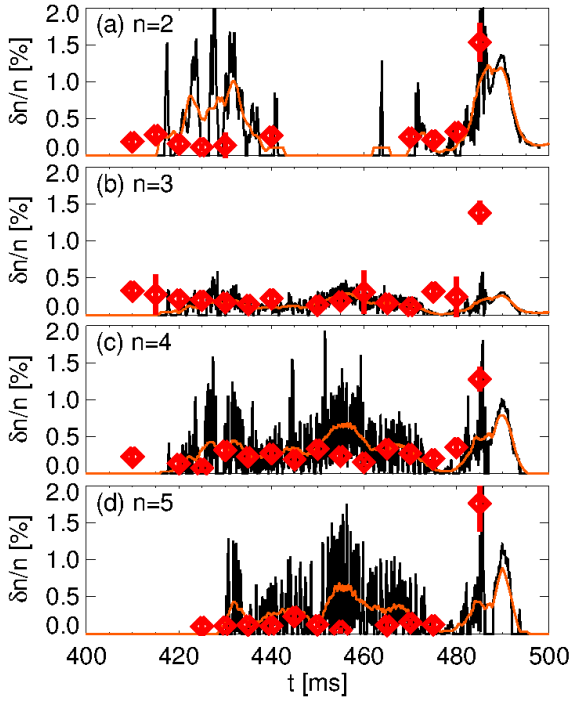

FIG. 15: Same as in Fig. 13 for density fluctuations from the kick model. Here, mode amplitudes are obtained by iterating TRANSP runs to achieve a good match between simulated and measured neutron rate. The solid red line represents a running average of the bursting amplitudes.

The peak density perturbation $\delta n/n$ associated with the iterated mode amplitudes is shown in Fig. 15 for modes with $n = 2 - 5$. Overall, the values of $\delta n/n$ from the modeling are in qualitative agreement with the measured perturbations. Differences in the time evolution are observed. For example, the modeled amplitudes increase between 440 ms and 460 ms, then decrease until the TAE avalanche event around 485 ms. These features are not clearly observed in the experimental $\delta n/n$. In general, however, discrepancies remain within a factor ≈ 2 or better over most of the simulation time range, which can be considered a satisfactory result for the reduced kick model.

TRANSP results with the updated mode amplitude waveforms for the kick model analysis are shown in Fig. 16 for the two sets of TAE modes previously selected (cf. Fig. 8) and for the amplitudes obtained after iterations. The simulations for the two sets of modes closely resemble those obtained with quasi-stationary mode amplitudes from the kick model. The only exception is the radial fast ion density profile (Fig. 16d), which does not show the core peaking as a result of the inclusion of the small $n = 1$ component. Finally, iterations on the mode amplitudes lead to TRANSP runs where a satisfactory match is obtained between measured and computed target quantity (in this case, the neutron rate). Those runs can then be used as starting point for further

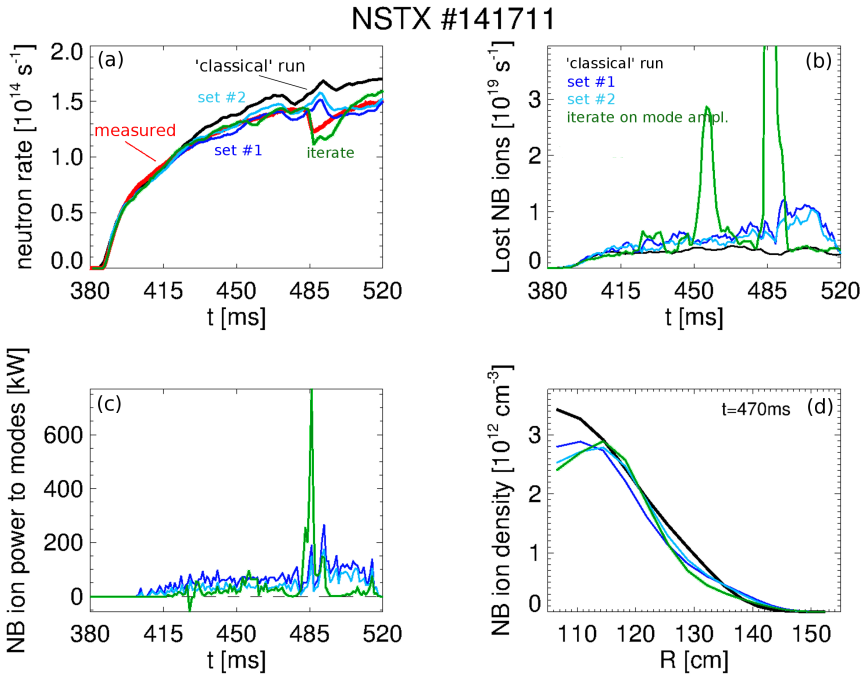

FIG. 16: TRANSP results for NSTX #141711 using the two sets of modes from Fig.7. Amplitudes for the two sets are taken from Mirnov coils measurements and re-scaled by the saturated amplitudes in Fig. 7. Amplitudes for curves in green are obtained by iterating on A_{mode} waveforms to match the measured neutron rate. (a) Neutron rate for the different Runs, also showing the measured values (red curve) and predictions for TRANSP run with *classical* fast ion transport (black) as reference. (b) Computed fast ion losses. (c) Total power transferred from fast ions to the modes. (d) Radial fast ion density profiles at $t = 470$ ms.

analysis, e.g. to infer transport levels, modifications to the fast ion distribution and NB current drive and its efficiency.

V. CONCLUSIONS

A reduced fast ion transport model (*kick model*), implemented in the time-dependent TRANSP code, has been used to predict stability properties of Alfvénic instabilities for the challenging regime encountered on NSTX. For a given set of thermal plasma profiles, estimates of the linear growth rate and saturation amplitude of the modes are obtained from a power balance between fast ion population and the instabilities. For the growth rate, values obtained from the kick model are consistent with NOVA results if finite Larmor radius effects are neglected, as expected since kick model probabilities are computed through ORBIT calculations based on gyro-center particle trajectories.

When compared with experimental data, kick model predictions, e.g. in terms of reduction in neutron rate, appear qualitatively consistent with the experiment and quantitatively satisfactory. The unstable TAE spectrum can be reproduced, although with a frequency shift (from NOVA analysis) with respect to the experiment. Predicted saturation amplitudes are within a factor two of the measured ones, which can be considered satisfactory given the uncertainties that propagate from the initial NOVA/ORBIT analysis to the inferred transport probabilities, hence to the kick model analysis.

If additional information from the experiment is used to further tune the kick model's parameters, a good agreement between TRANSP simulations and the experiment is achieved (e.g. in terms of neutron rate). This *interpretive* application of the model also provides improved match between measured and simulated fluctuation amplitudes.

The capability of the kick model - coupled to TRANSP - to perform time-dependent numerical experiments, e.g. for scenario development, has been discussed and will be further explored in following studies. More detailed validation of the kick model is also progressing. Although in the present work comparisons have been mainly based on the measured and simulated neutron rate, additional fast ion diagnostics can provide data for a more stringent validation. This effort has recently started (see, for instance, Ref. [27]) and the results will be presented in a future publication.

Acknowledgments

The support of the NSTX Team to run the experiments and provide the data required for this work is gratefully acknowledged, in particular the contribution of the NSTX Neutral Beam group and of Drs. B. LeBlanc, R. E. Bell, E. D. Fredrickson, S. P. Gerhardt and G. J. Kramer (PPPL); Drs. N. A. Crocker and S. Kubota (UCLA); Dr. H. Yuh (Nova Photonics). This material is based upon work supported by the U.S. Department of Energy, Office of Science, Office of Fusion Energy Sciences under contract number DE-AC02-09CH11466. NSTX at Princeton Plasma Physics Laboratory is a DOE Office of Science User Facility. The digital data for this paper can be found following the links from http://arks.princeton.edu/ark:/88435/dsp018p58pg29j.

---

[1] A. Fasoli, C. Gormezano, H. L. Berk, B. N. Breizman, S. Briguglio, D. S. Darrow, N. N. Gorelenkov, W. W. Heidbrink, A. Jaun, S. V. Konovalov, R. Nazikian, J.-M. Noterdaeme, S. Sharapov, K. Shinoara, D. Testa, K. Tobita, Y. Todo, G. Vlad, and F. Zonca, Nucl. Fusion **47**, S264 (2007)

[2] S. Sharapov, B. Alper, H. Berk, D. Borba, B. Breizman, C. Challis, I. Classen, E. Edlund, J. Eriksson, A. Fasoli, E. Fredrickson, G. Fu, M. Garcia-Munoz, T. Gassner, K. Ghantous, V. Goloborodko, N. Gorelenkov, M. Gryaznevich, S. Hacquin, W. Heidbrink, C. Hellesen, V. Kiptily, G. Kramer, P. Lauber, M. Lilley, M. Lisak, F. Nabais, R. Nazikian, R. Nyqvist, M. Osakabe, C. P. von Thun, S. Pinches, M. Podesta, M. Porkolab, K. Shinohara, K. Schoepf, Y. Todo, K. Toi, M. V. Zeeland, I. Voitsekhovich, R. White, V. Yavorskij, I. E. TG, and J.-E. Contributors, Nucl. Fusion **53**, 104022 (2013)

[3] N. N. Gorelenkov, S. D. Pinches, and K. Toi, Nucl. Fusion **54**, 125001 (2014)

[4] L. Chen and F. Zonca, Rev. Mod. Phys. **88**, 015008 (2016)

[5] K. Ghantous, N. N. Gorelenkov, H. L. Berk, W. W. Heidbrink, and M. A. Van Zeeland, Phys. Plasmas **19**, 092511 (2012)

[6] R. E. Waltz, E. M. Bass, W. W. Heidbrink, and M. Van Zeeland, Nucl. Fusion **55**, 123012 (2015)

[7] N. N. Gorelenkov, W. W. Heidbrink, G. J. Kramer, J. B. Lestz, M. Podestà, M. A. Van Zeeland, and R. B. White, Nuclear Fusion **56**, 112015 (2016)

[8] M. Podestà, M. Gorelenkova, and R. B. White, Plasma Phys. Control. Fusion **56**, 055003 (2014)

[9] For more details on the TRANSP code, please refer to the TRANSP webpage at http://w3.pppl.gov/˜pshare/help/transp.htm

[10] M. Ono, S. M. Kaye, Y.-K. M. Peng, G. Barnes, W. Blanchard, M. D. Carter, J. Chrzanowski, L. Dudek, R. Ewig, D. Gates, R. E. Hatcher, T. Jarboe, S. C. Jardin, D. Johnson, R. Kaita, M. Kalish, C. E. Kessel, H. Kugel, R. Maingi, R. Majeski, J. Manickam, B. McCormack, J. Menard, D. Mueller, B. Nelson, B. Nelson, C. Neumeyer, G. Oliaro, F. Paoletti, R. Parsells, E. Perry, N. Pomphrey, S. Ramakrishnan, R. Raman, G. Rewoldt, J. Robinson, A. L. Roquemore, P. Ryan, S. Sabbagh, D. Swain, E. J. Synakowski, M. Viola, M. Williams, J. R. Wilson, and NSTX Team, Nucl. Fusion **40**, 557 (2000)

[11] M. Podestà, R. E. Bell, N. A. Crocker, E. D. Fredrickson, N. N. Gorelenkov, W. W. Heidbrink, S. Kubota, B. P. LeBlanc, and H. Yuh, Nucl. Fusion **51**, 063035 (2011)

[12] M. Podestà, R. E. Bell, A. Bortolon, N. A. Crocker, D. S. Darrow, A. Diallo, E. D. Fredrickson, G. Fu, N. N. Gorelenkov, W. W. Heidbrink, G. J. Kramer, S. Kubota, B. P. LeBlanc, S. S. Medley, and H. Yuh, Nucl. Fusion **52**, 094001 (2012)

[13] E. D. Fredrickson, N. A. Crocker, R. E. Bell, D. S. Darrow, N. N. Gorelenkov, G. J. Kramer, S. Kubota, F. M. Levinton, D. Liu, S. S. Medley, M. Podestà, K. Tritz, R. B. White, and H. Yuh, Phys. Plasmas **16**, 122505 (2009)

[14] E. D. Fredrickson, N. A. Crocker, D. S. Darrow, N. N. Gorelenkov, G. J. Kramer, S. Kubota, M. Podestà, R. B. White, A. Bortolon, S. P. Gerhardt, R. E. Bell, A. Diallo, B. P. LeBlanc, F. M. Levinton, and H. Yuh, Nucl. Fusion **53**, 013006 (2013)

[15] R. J. Goldston, D. C. McCune, H. H. Towner, S. L. Davis, R. J. Hawryluk, and G. L. Schmidt, J. Comput. Phys. **43**, 61 (1981)

[16] A. Pankin, D. McCune, R. Andre, G. Bateman, and A. Kritz, Computer Physics Communication **159**, 157 (2004)

[17] R. B. White, The theory of toroidally confined plasmas, 2nd ed. (Imperial College Press, London, UK, 2006)

[18] R. B. White and M. S. Chance, Phys. Fluids **27**, 2455 (1984)

[19] C. Z. Cheng, Phys. Rep. 211 **1** (1992)

[20] G. Y. Fu and C. Z. Cheng, Phys. Fluids B **4**, 3722 (1992)

[21] N. N. Gorelenkov, C. Z. Cheng, and G. Y. Fu, Phys. Plasmas **6**, 2802 (1999)

[22] M. Podestà, M. Gorelenkova, E. D. Fredrickson, N. N. Gorelenkov, and R. B. White, Nuclear Fusion **56**, 112005 (2016)

[23] M. Podestà, M. Gorelenkova, E. D. Fredrickson, N. N. Gorelenkov, and R. B. White, Phys. Plasmas **23**, 056106 (2016)

[24] H. L. Berk and B. N. Breizman, Phys. Fluids B **2**, 2246 (1993)

[25] F. Zonca, F. Romanelli, G. Vlad, and C. Kar, Phys. Rev. Lett. **74**, 698 (1995)

[26] Y. Todo, H. L. Berk, and B. N. Breizman, Nucl. Fusion **52**, 094018 (2012)

[27] W. W. Heidbrink, C. Collins, M. Podestà, G. J. Kramer, D. Pace, C. Petty, L. Stagner, M. Van Zeeland, R. B. White, and Y. Zhu, Phys. Plasmas(submitted 2016)

[28] H. L. Berk, R. R. Mett, and D. M. Lindberg, Phys. Fluids B **5**, 3969 (1993)

[29] The LRDFIT code has been developed at the Princeton Plasma Physics Laboratory (Princeton, NJ - USA) by Dr. J. E. Menard, see webpage at http://w3.pppl.gov/~jmenard/software/lrdfit/lrdfit-overview.htm

[30] F. M. Levinton and H. Yuh, Rev. Sci. Instr. **79**, 10F522 (2008)

[31] B. P. LeBlanc, Rev. Sci. Instr. **79**, 10E737 (2008)

[32] R. E. Bell, Phys. Plasmas, accepted for publication(2010)

[33] M. Podestà, N. N. Gorelenkov, R. B. White, E. D. Fredrickson, S. P. Gerhardt, and G. J. Kramer, Phys. Plasmas **20**, 082502 (2013)

[34] R. B. White, N. N. Gorelenkov, M. Gorelenkova, M. Podestà, S. Ethier, and Y. Chen, Plasma Phys. Control. Fusion **58**, 115007 (2016)

[35] J. E. Menard, S. Gerhardt, M. Bell, J. Bialek, A. Brooks, J. Canik, J. Chrzanowski, M. Denault, L. Dudek, D. A. Gates, N. Gorelenkov, W. Guttenfelder, R. Hatcher, J. Hosea, R. Kaita, S. Kaye, C. Kessel, E. Kolemen, H. Kugel, R. Maingi, M. Mardenfeld, D. Mueller, B. Nelson, C. Neumeyer, M. Ono, E. Perry, R. Ramakrishnan, R. Raman, Y. Ren, S. Sabbagh, M. Smith, V. Soukhanovskii, T. Stevenson, R. Strykowsky, D. Stutman, G. Taylor, P. Titus, K. Tresemer, K. Tritz, M. Viola, M. Williams, R. Woolley, H. Yuh, H. Zhang, Y. Zhai, A. Zolfaghari, and NSTX Team, Nucl. Fusion **52**, 083015 (2012)

[36] Y. Todo, M. A. Van Zeeland, and W. W. Heidbrink, Nuclear Fusion **56**, 112008 (2016)

[37] M. Zhou and R. B. White, Plasma Phys. Control. Fusion **58**, 125006 (2016)

[38] C. S. Collins, W. W. Heidbrink, M. E. Austin, G. J. Kramer, D. C. Pace, C. C. Petty, L. Stagner, M. A. Van Zeeland, R. B. White, Y. B. Zhu, and DIII-D team, Phys. Rev. Letters **116**, 095001 (2016)

[39] W. W. Heidbrink, C. Collins, L. Stagner, Y. B. Zhu, C. C. Petty, and M. Van Zeeland, Nucl. Fusion **56**, 112011 (2016)

[40] J. Park, R. J. Goldston, N. A. Crocker, E. D. Fredrickson, M. G. Bell, R. Maingi, K. Tritz, M. A. Jaworski, S. Kubota, and F. Kelly, Nucl. Fusion **54**, 043013 (2014)

[41] D. Liu, G. Fu, N. A. Crocker, M. Podestà, J. A. Breslau, E. D. Fredrickson, and S. Kubota, Phys. Plasmas **22**, 042509 (2015)

[42] S. Kubota, W. A. Peebles, X. V. Nguyen, N. A. Crocker, and A. L. Roquemore, Rev. Sci. Instr. **77**, 10E926 (2006)

[43] N. A. Crocker, W. A. Peebles, S. Kubota, J. Zhang, R. E. Bell, E. D. Fredrickson, N. N. Gorelenkov, B. P. LeBlanc, J. E. Menard, M. Podestà, S. A. Sabbagh, K. Tritz, and H. Yuh, Plasma Phys. Control. Fusion **53**, 105001 (2011)

[44] V. Duarte, H. Berk, N. N. Gorelenkov, W. W. Heidbrink, G. J. Kramer, R. Nazikian, D. Pace, M. Podestà, B. Tobias, and M. A. Van Zeeland, ???(submitted 2016)